ChemComm

Cite this: *Chem. Commun.*, 2011, **47**, 12173–12175

www.rsc.org/chemcomm

COMMUNICATION

Direct tuning of electrical properties in nano-structured $Bi_2Se_{0.3}Te_{2.7}$ by reversible electrochemical lithium reactions†

Jikun Chen,[a] Xiaoyuan Zhou,[b] G. Jeffrey Snyder,[c] Ctirad Uher,[b] Nuofu Chen,[d] Zhaoyin Wen,[a] Jun Jin,[a] Hongliang Dong,[a] Pengfei Qiu,[a] Yanfei Zhou,[a] Xun Shi*[a] and Lidong Chen*[a]

Received 5th September 2011, Accepted 6th October 2011
DOI: 10.1039/c1cc15498b

Lithium intercalation and de-intercalation processes have been used to fabricate bulk $Bi_2Se_{0.3}Te_{2.7}$ with internal nanostructures. The doped Li content can be precisely controlled through this method. It provides a chance to directly optimize electrical properties when preparing nano-structured materials, leading to the optimum carrier concentration for improved thermoelectric figure of merit.

Nano-structure designs provide an additional opportunity for further optimization of thermoelectric (TE) performance, which is evaluated by the dimensionless TE figure of merit ZT ($ZT = S^2\sigma T/\kappa$), where S is Seebeck coefficient, σ is electrical conductivity, T is absolute temperature, and κ is thermal conductivity.[1] Either low dimensional structures like superlattices and nano-wire arrays,[2,3] or internal nano-structures within three-dimensional bulk matrices such as nano-inclusions[4–9] and nano-crystals[10–14] could effectively decrease the lattice thermal conductivity (κ_L), resulting in the enhancement of ZT in many types of TE materials, *e.g.*, Bi_2Te_3, PbTe, SiGe, Skutterudites and even Si.[2] Nevertheless, except for the reduced κ_L, another aspect that should not be neglected to achieve optimum ZT values in nano-structured TE materials is the optimization of charge carrier concentration and electrical transport properties. In this communication, a novel three-step approach, involving a quick spark plasma sintering (SPS) technique and reversible electrochemical lithium intercalation and de-intercalation reactions, has been applied to prepare nano-structured $Bi_2Se_{0.3}Te_{2.7}$ TE material with well controlled carrier concentration, providing a direct opportunity to simultaneously optimize electrical and thermal properties during the synthesis of nano-structured TE materials.

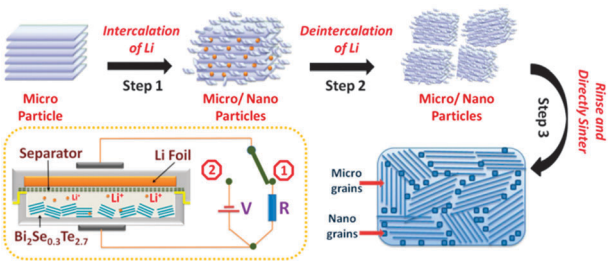

Scheme 1 Schematic illustration of fabrication of nano-structured composites using reversible electrochemical reactions. The inset shows the device structure used for electrochemical Li intercalation (switch in position 1) and de-intercalation (switch in position 2).

Similar to Bi_2Te_3, $Bi_2Se_{0.3}Te_{2.7}$ has hexagonal structure, consisting of five layered lamellas (called quintuples) in the form of [$Te^{(1)}$, $Se^{(1)}$]–Bi–[$Te^{(2)}$, $Se^{(2)}$]–Bi–[$Te^{(1)}$,$Se^{(1)}$]. Within each lamella, all the atoms are bonded covalently, but the neighboring quintuple layers are loosely held together by weak van der Waals bonds, which makes the intercalation of small atoms like lithium possible.[15–20] Scheme 1 illustrates the fabrication method. It contains three steps. The first one is to intercalate Li into the van der Waal gap between the connected [$Te^{(1)}$, $Se^{(1)}$]–[$Te^{(1)}$, $Se^{(1)}$] layers of micro-scaled $Bi_2Se_{0.3}Te_{2.7}$ powder using an electrochemical discharging process described in ref. 16 and ref. 22. In the second step, a reversed electrochemical lithium de-intercalation process was carried out by recharging the lithium cell using constant electrical currents to pull out a controlled amount of inter-calated Li atoms from $Bi_2Se_{0.3}Te_{2.7}$. Finally, the obtained $Bi_2Se_{0.3}Te_{2.7}$ micro- and nano-scale composite scaled powders with a controlled residual lithium content were taken out of the cell, rinsed in acetone and sintered into bulk nano-structured material using spark plasma sintering (SPS).

Fig. 1a shows the cyclic voltammogram of the reversed electrochemical lithium intercalation and de-intercalation reactions with $Bi_2Se_{0.3}Te_{2.7}$ (see the lithium intercalation and deintercalation curves in Fig. S1, ESI†). During the lithium intercalation and de-intercalation processes, the surface layer of original micro-scaled powder has been exfoliated into nano-scaled $Bi_2Se_{0.3}Te_{2.7}$ particles with scale around 10 nm (see more details in Fig. S2 and S3, ESI†). By following SPS,

[a] *CAS Key laboratory of Materials for Energy Conversion, Shanghai Institute of Ceramics, Chinese Academy of Science, Shanghai 200050, China. E-mail: chenlidong@mail.sic.ac.cn*
[b] *Department of Physics, University of Michigan, Ann Arbor, Michigan 48109, USA*
[c] *Materials Science, California Institute of Technology, Pasadena, CA 91125, USA*
[d] *School of Renewable Energy, North China Electric Power University, Beijing 102206, China*
† Electronic supplementary information (ESI) available. See DOI: 10.1039/c1cc15498b

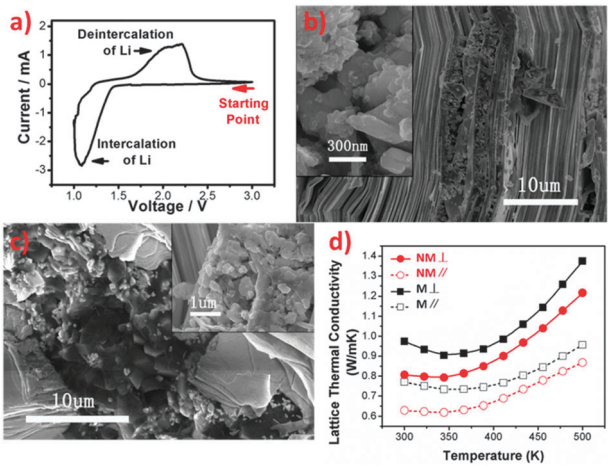

Fig. 1 (a) Cyclic voltammogram of reversible lithium reactions with $Bi_2Se_{0.3}Te_{2.7}$ (with scanning speed of 50 mV s^{-1}, and scope of 1 V–3 V). (b), (c) SEM images of fractured surface morphologies both parallel (b) and perpendicular (c) to SPS pressure in nano-/micro-composite crystalline bulk $Li_{0.11}Bi_2Se_{0.3}Te_{2.7}$ (the insets show morphologies of the nano-scaled grains with larger magnification). (d) Lattice thermal conductivity of as-fabricated nano/micro composite crystalline $Li_{0.11}Bi_2Se_{0.3}Te_{2.7}$ (**NM**) in directions both perpendicular (⊥) and parallel (∥) to SPS pressure, compared with $Bi_2Se_{0.3}Te_{2.7}$ samples SPSed using pristine micro-powders under same conditions (**M**).

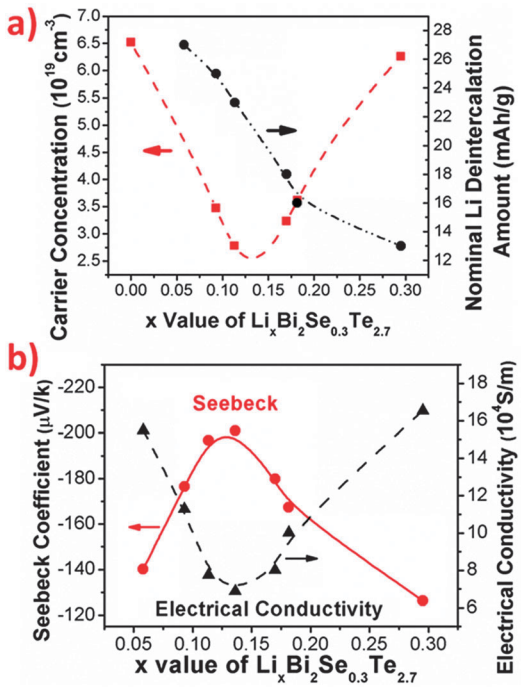

Fig. 2 (a) Carrier concentrations as a function of Li content at 300 K, together with the relationship between residual Li content (x) measured by Inductively Coupled Plasma Optical Emission Spectrometry (ICP-OES) in nano-structured $Bi_2Se_{0.3}Te_{2.7}$ and nominal de-intercalation lithium amount (fixing intercalation lithium amount as 25 mAh g^{-1}); (b) Seebeck coefficient and electrical conductivity as a function of Li content at 300 K.

a sandwich-like nano/micro composite crystalline structure, in which nano-scaled grains sandwiched within the laminars of micro-scaled grains, has been obtained. Fig. 1b and c show its SEM image of fractured surface morphology both parallel and perpendicular to the SPS pressure (see XRD patterns along both directions in Fig. S4, ESI†). This structure could more effectively scatter lattice phonons. Significant decrease in κ_L has been achieved in both along and perpendicular to the sintering pressure directions, as shown in Fig. 1d (see more detailed thermal and electrical transportation properties in Fig. S5, ESI†).

Fixing the intercalated Li amount in the first step, the actual residual Li content (marked as x) in $Li_xBi_2Se_{0.3}Te_{2.7}$ could be well controlled by the de-intercalation process during the second step. Fig. 2a shows the relationship between measured actual x value (by ICP-OES) and the nominal lithium de-intercalation amount (recharging current × recharging time). The actual residual lithium amount shows a decreasing trend with the increasing nominal deintercalation lithium amount. Usually the intercalated Li atoms in $Bi_2Se_{0.3}Te_{2.7}$ donate their valence charges into the matrix crystal, which could be used to tune the carrier concentration and thereby electrical properties in these nano-structured $Bi_2Se_{0.3}Te_{2.7}$ samples.

The measured room temperature carrier concentration is shown in Fig. 2a. An unusual non-monotonic trend is observed when changing the Li content, while it should monotonically increase if only the effect of intercalated Li is accounted. Table 1 further compares the carrier concentration and carrier mobilities of $Li_xBi_2Se_{0.3}Te_{2.7}$ samples with various residual lithium contents at 300 K. This abnormal behavior of carrier concentration variation could be explained by a readjustment of Bi–Te (or Se) anti-site defect concentration, which also affects the carrier concentration in bismuth chalcogenide compounds.[21] Our original $Bi_2Se_{0.3}Te_{2.7}$ sample shows that the dominated carriers are electrons due to the deficient Se or Te atoms in the lattice. The intercalated Li atoms in $Bi_2Se_{0.3}Te_{2.7}$ are believed to more easily bond with Se atoms because of their highest electronegativity value among elements Bi, Se, and Te. In order to accept more Li atoms during electrochemical reactions, the amount of Se defects is reduced in the mixed nano- and micro-powders, leading to the lowered electron concentration. The Se defects are reduced quickly and finally saturated when increasing the intercalated Li atoms. The measured electron concentrations are thereby dominated by the Li content, leading to a continually enhanced electron concentration (see Fig. 2a and Table 1).

Two opposite mechanisms to adjust the carrier concentration are at play here: intercalated Li atoms donating electrons, and reduced density of Se defects generating holes. Combining the above two effects, we can directly optimize both electrical and thermal properties in nano-structured $Bi_2Se_{0.3}Te_{2.7}$. Fig. 2b shows the data of σ and S at 300 K.

Table 1 Hall measurement for $Li_xBi_2Se_{0.3}Te_{2.7}$ fabricated through lithium intercalation/de-intercalation reactions at 300 K

x Value in $Li_xBi_2Se_{0.3}Te_{2.7}$	Carrier concentration (10^{19} cm^{-3})	Carrier mobility (cm^2 V^{-1} S^{-1})
0 (Orig.)	6.52	195
0.09	3.47	179
0.11	2.78	168
0.18	3.62	166
0.30	6.26	155

Similar to electron concentration, S (or σ) initially increases (or decreases) in magnitude when x values are from 0.05 to 0.15. When x is larger than 0.15, absolute S (or σ) gradually decreases (or increases). For x around 0.15, the lowest carrier concentration and electrical conductivity, and the highest absolute S are obtained; leading to an enhancement of the maximum ZT of more than 20% (see Fig. S5, ESI†).

In summary, a new three-step approach, based on reversible electrochemical lithium reactions, has been demonstrated to fabricate bulk $Bi_2Se_{0.3}Te_{2.7}$ with internal nanostructure. The doped Li content can be well controlled to realize optimum carrier concentration for electrical properties and TE performance.

Financial support from Program of Shanghai Subject Chief Scientist (No. 09XD1404400), and National Basic Research Program of China (973 Program) (No.2007CB607500) is gratefully acknowledged. The work at the University of Michigan (low temperature Hall effect and resistivity) is supported as part of *Revolutionary Materials for Solid State Energy Conversion*, an Energy Frontier Research Center funded by the U.S. Department of Energy, Office of Basic Energy Sciences under Award DE-SC0001054. Financial support from National High Technology Research and Development Program (“863”Program) of China under contract: 2011AA050507 is also gratefully acknowledged.

Notes and references

1 M. S. Dresselhaus, G. Chen, M. Y. Tang, R. G. Yang, H. Lee, D. Z. Wang, Z. F. Ren, J. P. Fleurial and P. Gogna, *Adv. Mater.*, 2007, **19**, 1043.
2 A. L. Hochbaum, R. K. Chen, R. D. Delgado, W. J. Liang, E. C. Garnett, M. Najarian, A. Majumdar and P. D. Yang, *Nature*, 2008, **451**, 163.
3 T. C. Harman, P. J. Taylor, M. P. Walsh and B. E. La Forge, *Science*, 2002, **297**, 27.
4 K. F. Hsu, S. Loo, F. Guo, W. Chen, J. S. Dyck, C. Uher, T. Hogan, E. K. Polychroniadis and M. G. Kanatzidis, *Science*, 2004, **303**, 818.
5 Y. Pei, J. Lensch-Falk, E. S. Toberer, D. L. Medlin and G. J. Snyder, *Adv. Funct. Mater.*, 2010, **21**, 241.
6 H. Li, X. Tang, Q. Zhang and C. Uher, *Appl. Phys. Lett.*, 2009, **94**, 102114.
7 Z. Xiong, X. Chen, X. Huang, S. Bai and L. Chen, *Acta Mater.*, 2010, **58**, 3995.
8 W. J. Xie, X. F. Tang, Y. G. Yan, Q. J. Zhang and T. M. Tritt, *Appl. Phys. Lett.*, 2009, **94**, 102111.
9 D. Teweldebrhan, V. Goyal, M. Rahman and A. A. Balandin, *Appl. Phys. Lett.*, 2010, **96**, 053107.
10 X. B. Zhao, X. H. Ji, Y. H. Zhang, T. J. Zhu, J. P. Tu and X. B. Zhang, *Appl. Phys. Lett.*, 2005, **86**, 062111.
11 G. H. Dong, Y. J. Zhu and L. D. Chen, *J. Mater. Chem.*, 2010, **20**, 1976.
12 M. Scheele, N. Oeschler, K. Meier, A. Kornowski, C. Klinke and H. Weller, *Adv. Funct. Mater.*, 2009, **19**, 3476.
13 B. Poudel, Q. Hao, Y. Ma, Y. C. Lan, A. Minnich, B. Yu, X. Yan, D. Z. Wang, A. Muto, D. Vashaee, X. Y. Chen, J. M. Liu, M. S. Dresselhaus, G. Chen and Z. F. Ren, *Science*, 2008, **320**, 634.
14 Y. Lan, A. J. Minnich, G. Chen and Z. Ren, *Adv. Funct. Mater.*, 2010, **20**, 357.
15 Z. F. Ding, L. Viculis, J. Nakawatase and R. B. Kaner, *Adv. Mater.*, 2001, **13**, 797.
16 J. K. Chen, Y. J. Zhu, N. F. Chen, Y. F. Zhou, J. Ding, X. H. Chen and L. D. Chen, *Dalton Trans.*, 2011, **40**, 340.
17 J. Bludská, S. Karamzov, J. Navrátil and J. Horák, *Solid State Ionics*, 2004, **171**, 251.
18 S. N. Chizhevskaya, T. E. Svechnikova, S. Y. Skipidarov, N. A. Tsvetkova and N. N. Nemtsov, *Inorg. Mater.*, 1992, **28**, 231.
19 J. Bludska, I. Jakubec, S. Karamazov, J. Horak and C. Uher, *J. Solid State Chem.*, 2010, **183**, 2813.
20 Z. F. Ding, S. K. Bux, D. J. King, F. L. Chang, T. H. Chen, S. C. Huang and R. B. Kaner, *J. Mater. Chem.*, 2009, **19**, 2588.
21 G. S. Nolas, J. Sharp and H. J. Goldsmid, *Thermoelectrics*, Springer, Berlin, 2001, p. 36.
22 J. K. Chen, Y. J. Zhu, N. F. Chen, X. L. Liu, Z. L. Sun, Z. H. Huang, F. Y. Kang, Q. M. Gao, J. Jiang and L. D. Chen, *J. Nanopart. Res.*, 2011, DOI: 10.1007/s11051-011-0563-0.